Microsc. Microanal. Page 1 of 9
doi:10.1017/S1431927613013718

Microscopy AND Microanalysis

Unusual Micrometric Calcite–Aragonite Interface in the Abalone Shell *Haliotis* (Mollusca, Gastropoda)

Yannicke Dauphin,[1,*] Jean-Pierre Cuif,[1] Hiram Castillo-Michel,[2] Corinne Chevallard,[3] Bastien Farre[1,4] and Anders Meibom[5]

[1]*UMR 8148 IDES, bât. 504, Université Paris Sud, 91405 Orsay cedex, France*
[2]*ID21, ESRF, BP 220, 6 rue J. Horowitz, 38043 Grenoble, France*
[3]*UMR SIS2M 3299, LIONS, CEA, 91191 Gif sur Yvette, France*
[4]*UMR 7327 ISTO, 1A rue de la férollerie, 45100 Orléans, France*
[5]*Laboratory for Biological Geochemistry, School of Architecture, ENAC, EPFL, 1015 Lausanne, Switzerland*

Abstract: Species of *Haliotis* (abalone) show high variety in structure and mineralogy of the shell. One of the European species (*Haliotis tuberculata*) in particular has an unusual shell structure in which calcite and aragonite coexist at a microscale with small patches of aragonite embedded in larger calcitic zones. A detailed examination of the boundary between calcite and aragonite using analytical microscopies shows that the organic contents of calcite and aragonite differ. Moreover, changes in the chemical composition of the two minerals seem to be gradual and define a micrometric zone of transition between the two main layers. A similar transition zone has been observed between the layers in more classical and regularly structured mollusk shells. The imbrication of microscopic patches of aragonite within a calcitic zone suggests the occurrence of very fast physiological changes in these taxa.

Key words: biominerals, mollusk shells, aragonite, calcite, FTIR, NanoSIMS

Introduction

Mollusks are organisms characterized by important internal interfaces at a variety of levels (Boggild, 1930; Taylor et al., 1969). The first interface level is defined at the macroscale where mantle cells are in contact with the carbonate shell they form (Fig. 1a). A second mesoscale interface exists within the shells, which are composed of several layers of variable structure and/or mineralogy (Fig. 1b). At the microscale, an organo-mineral interface level exists within each layer where crystalline units are surrounded by organic envelopes (Fig. 2c, arrow). Within an individual crystalline unit, another organo-mineral interface exists because rounded nanogranules are surrounded by a cortex probably composed of a mixture of amorphous calcium carbonate and organics (Fig. 1d, star). Nanogranules are themselves a mixture of organic and minerals, as shown by color variations in atomic force phase image (Fig. 1c). And finally, a molecular-level interface has been shown: the organic matrices extracted from the crystalline units are a mixture of proteins, sugars (Figs. 1e, 1f), and lipids (Farre et al., 2011).

The shells produced by mollusks are made of calcium carbonate in the form of aragonite and/or calcite. In most shells, calcite and aragonite are arranged in regular layers, the limits of which are parallel to the outer surface of the shell. Because of their spiral shell morphology, gastropods are not the most studied shells. However, some species have shells with a reduced coiling in which only the apex has a spiral shape. Among them is *Haliotis* (abalone), a popular seafood, with a shell up to 25 cm long, living in shallow water underneath weed-covered rocks and boulders to depths of about 40 m in oceans worldwide. As an aside, this slow moving gastropod is easy to catch so that overfishing, based exclusively on the extraction of wild stocks, has threatened the species in several countries (Japan, Australia, California, South Africa, France, etc.). An official ban on ormer fishing has been imposed in the countries mainly concerned because of the severe drop in the yields (Clavier, 1982).

Haliotis comprises more than 100 species, each with a specific microstructural arrangement. The shell is usually bilayered with an inner aragonitic nacreous layer and an outer prismatic layer. Depending of the species, the outer layer is either calcite or aragonite. This unusual variability was noticed as early as 1930 (Boggild, 1930): they "possess, in some instances, a calcitic layer inserted between two aragonitic ones. . . The calcite has a rather regularly prismatic structure." Kessel (1935), using specific stains, noted that in *Haliotis tuberculata*, aragonite and calcite are not separated into distinct layers and that numerous aragonitic granules are imbricated in calcitic prisms. The imbricated structure of *H. tuberculata* as well as *Haliotis lamellosa* was confirmed by scanning electron microscope (SEM) observations (Mutvei et al., 1985; Dauphin et al., 1989): the inner nacreous layer is aragonitic, whereas the middle layer is mainly prismatic calcite, the outer layer being prismatic aragonite. A similar arrangement also exists in *Haliotis discus* and *Haliotis roei* (Fig. 2). Thus, the two prismatic layers have different mineralogies, while the two aragonitic layers have distinct microstructures. Only *in situ* localized analyses are suitable to improve our knowledge of the structure and composition of individual layers, and to understand the biomineralization mechanisms of such com-

Received April 26, 2013; accepted September 30, 2013
*Corresponding author. E-mail: yannicke.dauphin@u-psud.fr

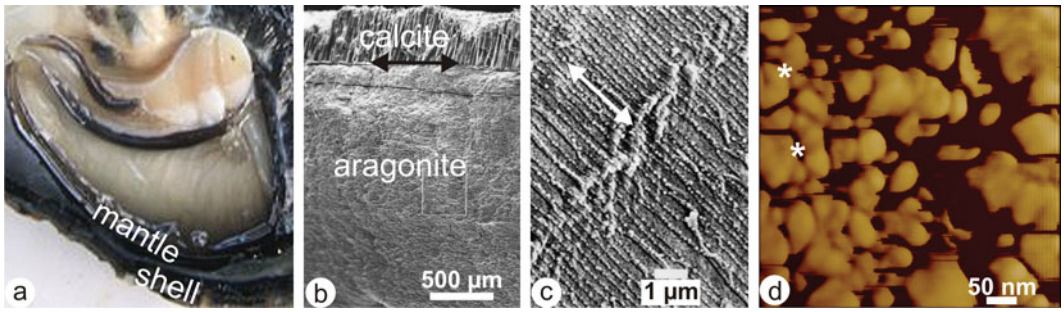

Figure 1. Multiscale interfaces in mollusk shells. **a:** Inner view of the pallial cavity of *Pinctada* showing the macroscale interface between the mantle cells and the shell. **b:** Vertical section of a shell of *Pinctada* showing the interface between two different structural and mineralogical layers. **c:** Section of a nacreous layer of *Haliotis* showing the microscale interface between the tablets and their organic envelopes (arrow). **d:** Nanoscale interfaces between the rounded granules with a cortex (star), and within the organo-mineral granules; *Neotriginia* shell.

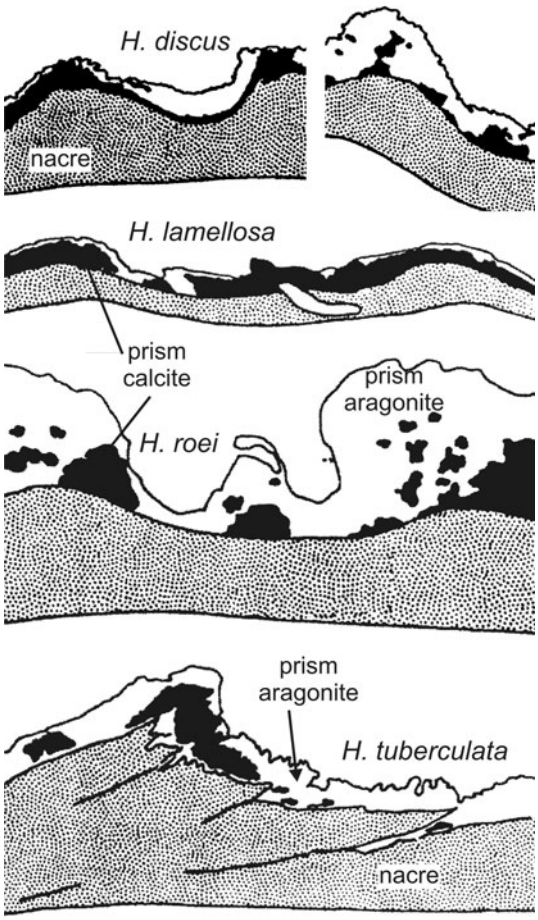

Figure 2. Vertical shell sections of four *Haliotis* species, showing the irregular layering of the calcite (black) and aragonite (white) "prismatic" layer in the outer part of the shell. In all species, the inner layer is the aragonitic nacre. Redrawn from Mutvei et al. (1985).

plex shells. Electron microprobe analyses have shown that the magnesium (Mg) contents of the calcitic layers are low but differ (from 800 ppm in *Haliotis kamtschakana* to 3,800 ppm in *Haliotis rotundata*). Analyses of ten species have also shown that strontium (Sr) contents of the aragonitic prismatic and nacreous layers are also low and different in a given species (Dauphin et al., 1989), but both calcite and aragonite compositions in these two species fall within the broad range of compositions defined by mollusk shells in general.

In complex shells such as *H. tuberculata* or *H. roei*, bulk separation of the distinct shell components is not possible, making a reliable investigation of their respective chemical and biochemical compounds very difficult by conventional methods. *In situ* characterizations of biochemical compounds have proven efficient methods in previous studies. Synchrotron-based XANES mapping, for instance, has demonstrated that sulfur is mainly associated with sulfated sugars, and that calcite layers have higher contents (Dauphin et al., 2005). The focus of the current investigation is to determine the spatial and chemical relationship between aragonite and calcite at a microscale in the outer layer of *Haliotis*.

Materials and Methods

Material

Haliotis (Gastropoda, Orthogastropoda, Pleurotomaroidea, Haliotidae) has more than 100 species and a worldwide distribution.

H. tuberculata Linnaeus, 1758 were obtained from the Station Biologique de Dinard (France) in the English Channel. *H. tuberculata* is present in the Channel Isles but absent from the coasts of Britain and Ireland. *H. lamellosa* Lamarck, 1822 is usually considered as a subspecies of *H. tuberculata*. Shells were collected in the Mediterranean Sea.

H. tuberculata has a flattened, oval shell, up to 9 cm long and 6.5 cm large, slightly coiled at the apex (Fig. 3). A row of round respiratory holes runs along the bottom margin of the shell. The outer, larger (from five to seven) holes are open while the older are closed. The outer surface of the shell is greenish-brown to red (Figs. 3a, 3c). The inner surface is lined with an iridescent nacreous layer (= mother-of-pearl) (Figs. 3b, 3d).

Optical Microscopy

Thin sections were observed under crossed Nicols in transmitted light.

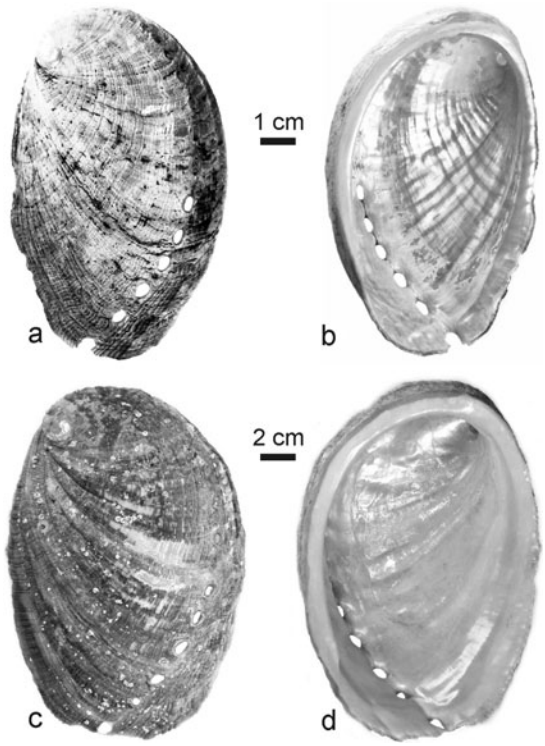

Figure 3. Juvenile (**a, b**) and adult (**c, d**) shells of *Haliotis tuberculata*. The outer surfaces of these cultivated samples are unusually clean, devoid of encrusting epibionts. **a, c:** Outer surfaces. **b, d:** Inner surface showing the nacreous layer.

The epifluorescence signal of polished surfaces was observed under ultraviolet (UV) light using a Zeiss Standard microscope (Carl Zeiss, Jena, Germany) equipped with Neofluor fluorine objectives, a Zeiss mercury lamp, excitation filter (365 nm), and transmission cut-off filter (400 nm).

A second set of observations was conducted at the LIONS laboratory (CEA Saclay, DSM/IRAMIS/SIS2M) on an Olympus FV1000 confocal microscope (Olympus Corporation, Tokyo, Japan). All the samples examined had been previously sectioned and polished to a smooth surface. A 60× oil-immersion objective was used in order to achieve the best achievable spatial resolution (~200 nm horizontal resolution). Two different excitation wavelengths were used, namely the 488 nm laser line of an Argon laser and the 633 nm line of a He–Ne laser, and the emitted fluorescence signal was collected in the range 515–545 nm and above 650 nm, respectively.

SEM

A Philips 505 SEM, a Philips XL30, and a Phenom Pro X (Université Paris Sud) were used to obtain images of the features within the etched and polished samples. Various etching and/or fixative procedures were used to reveal the details of the microstructures of the prismatic layers. Bacteria were used to remove the organic matrices, formic and acetic acids were used to etch the carbonate. Actually, bacterial etchings partially dissolved the minerals, whereas acids partially etched the organic matrices. So some fixatives such as glutaraldehyde, or fixative-etching agent such as chromium sulfate were used to fix the organic matrix. Details of the etching procedures are given in the figure captions.

Fourier Transform Infrared Microscopy (FTIR)

The synchrotron infrared microscopy was performed on the FTIR end station of the ID21 beam line at the European Synchrotron Radiation Facility (ESRF). This beam line is equipped with a Continuum IR microscope (Thermo Nicolet, Thermo Fisher Scientific, Inc., Waltham, MA, USA) coupled to a Nexus FTIR bench (Thermo Nicolet). The microscope can be operated in confocal or reflection mode, where the focusing Schwarzschild objective and the collection Schwarzschild objective have a magnification of 32× (NA = 0.65). Due to its reduced source size and high collimation properties, a synchrotron infrared source is more efficiently coupled to the low acceptance of the confocal microscope, while its higher spectral luminescence (brightness) allows signal-to-noise ratios to be kept at diffraction-limited resolutions. The microscope is equipped with a computer-controlled x/y stage allowing acquisition of profiles or maps of the sample. Maps were scanned with steps of 4 μm in both directions, with an aperture size of 5×5 μm^2. Spectra were collected in reflection mode, with a resolution of 8 cm^{-1}. For each spectrum, 100 scans were accumulated in the wavenumber range 4,000–700 cm^{-1}. Polished and cleaned surfaces were prepared as for the first step of SEM observations, without etching. The final format of the data were recorded as absorbance values.

NanoSIMS

Samples were cut perpendicular to the interface between the nacre and the prismatic layer, mounted in epoxy (Körapox©) and polished to a 0.25 mm finish using diamond paste. The samples were then gold coated. Chemical mapping was carried out with the Cameca NanoSIMS N50 at the Muséum National d'Histoire Naturelle in Paris, following established procedures for biogenic carbonates (Meibom et al., 2004, 2008; Brahmi et al., 2010; Kopp et al., 2011).

Briefly, using a focused primary beam of O^- to a spot size of about 250 nm, secondary ions of $^{24}Mg^+$, $^{44}Ca^+$, and $^{88}Sr^+$ were sputtered from the sample surface and detected simultaneously (in multicollection mode) using electron multipliers. The mass-resolving power was ~4,000 ($M/\Delta M$), sufficient to resolve all isobaric interferences. Chemical maps were obtained by rastering the primary beam across a selected and presputtered sample surface.

Results

Structure

Three structural types build the shell of *H. tuberculata*. These structures are not regular layers with boundaries parallel to the inner and/or outer surface of the shell. UV optical images show the different auto-fluorescence of the three structures (Figs. 4a). Despite the fact that nacre and the outer layers are aragonite, intensities and colors differ.

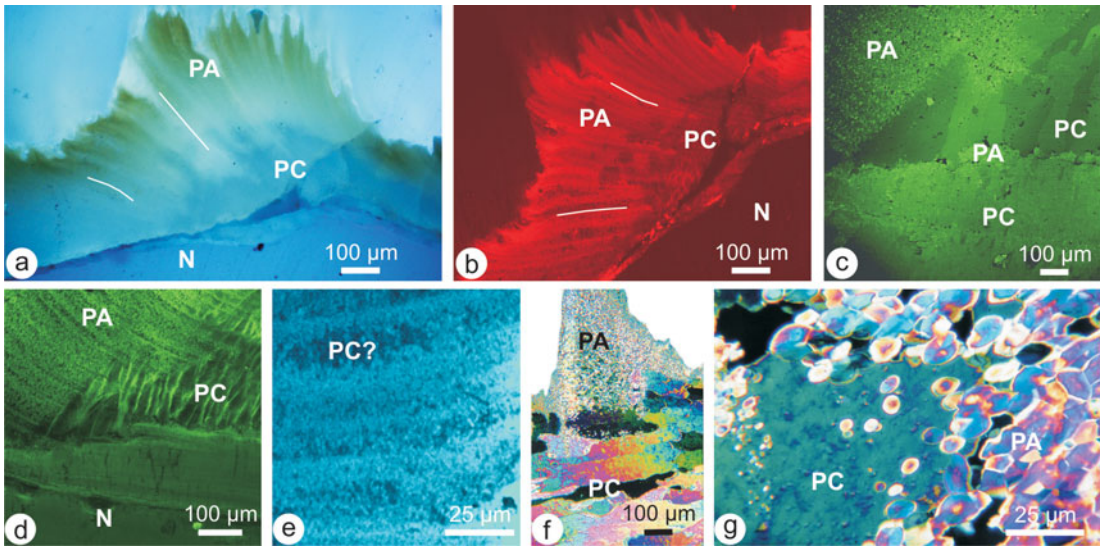

Figure 4. **a:** Fluorescence image (UV excitation) showing the differential response of the three structures. **b:** Laser confocal image showing differences in the three structures of the shell of *Haliotis tuberculata*, and the banding pattern of the prismatic–spherulitic aragonite; laser wavelength 633 nm. **c:** Laser confocal image: detail showing the calcitic prisms and the "granular" aspect of the aragonitic outer layer; laser wavelength 488 nm. **d:** Laser confocal image showing the organic envelope surrounding the calcitic prisms and the growth layer in the external aragonite; laser wavelength 488 nm. **e:** Detail showing a small patch of calcite in the aragonitic layer; laser wavelength 488 nm. **f:** Polarized crossed Nicols image showing the small aragonitic units and the large calcitic prisms. **g:** Polarized cross Nicols image showing the various size of the small aragonitic units within a calcitic crystal. PC, prismatic calcite; PA, prismatic–spherulitic aragonite; N, nacreous layer.

Confocal laser images also show the distinct response of the structures (Figs. 4b–4e). Growth layers are clearly visible in the outer aragonitic prisms, whereas the nacreous layer seems to be homogeneous (Fig. 4b). A green excitation wavelength emphasizes the shape of the calcitic prisms, the irregular distribution of the aragonitic prisms (Figs. 4c, 4d), and the organic envelopes of the calcitic prisms (Fig. 4d). Larger magnifications show the granular structure and growth layers in the aragonitic layer (Fig. 3e). The small darker zone may correspond to calcitic prisms embedded in the aragonitic zone (Fig. 4e). Transmitted crossed Nicols images of thin sections show the large size of the calcitic prisms and the small aragonitic units (Figs. 4f, 4g). A larger magnification shows that calcite and aragonite are produced simultaneously at a microscale (Fig. 4g).

SEM confirms the irregular distribution of the calcite and aragonite in the outer part of the shell (Figs. 5a–5c). The outermost part of the shell is an irregular arrangement of small aragonitic prisms or spherulites, containing patches of calcitic prisms (Figs. 5a–5g). The individual spatial distribution of calcite and aragonite, as well as the size of the calcitic patches, vary substantially. However, the most external part of the shell is always aragonite. The calcite is between prismatic–spherulitic aragonite and the inner aragonitic nacre, but has a very irregular thickness and presence (Figs. 5a–5c). The structural differences between aragonite and calcite of the external zone of the shell observed in fractured surfaces and polished sections show that small aragonitic spherulites are also dispersed in large calcite crystals (Figs. 5d, 5e). Etched and fixed sections or fractures show the organic framework of the aragonitic spherulites (Fig. 5f) and of the calcitic prisms. The inner structures of the aragonitic outer layer, the calcitic prismatic layer, and the nacreous layer are shown, respectively, in Figures 5g–5i.

Bulk Composition

FTIR maps have been acquired on a vertical section where aragonite and calcite are not in regular layers (Fig. 6). Spectra of the calcite and aragonite groups are characterized by three major bands attributed to the carbonate ion CO^{2-}_3: $\nu 3$ at 1,429 cm^{-1}, the $\nu 2$ doublet 877–848 cm^{-1}, and $\nu 4$ at 713 cm^{-1} for the calcite group; $\nu 3$ at 1,471 cm^{-1} and two doublets: $\nu 2$ at 858–844 cm^{-1} and $\nu 4$ at 713–700 cm^{-1} for the aragonite group (White, 1974). Map at 875 cm^{-1} displays the aragonitic and calcitic zones of the shell (Fig. 7). The characteristic $\nu 2$ absorption bands of calcite and aragonite can be observed in the infrared spectra extracted from a region where the map at 875 cm^{-1} shows a transition from calcite to aragonite in the shell structure (Fig. 7). In such organo-mineral assemblages, a precise assignment of FTIR bands is not possible because of the overlapping of bands. The 883 cm^{-1} band corresponds to various organic components with C–H and CH_2 bonds. Despite this vague assignment, the 883 cm^{-1} map clearly shows the difference in aragonite and calcite, whatever the structure (Fig. 7). Sugar bands are between 950 and 1,150 cm^{-1}, so that it can be suggested that the map at 1,148 cm^{-1} is related to these components. Again, aragonite and calcite are different, but nacre and outer aragonite are not identical. The

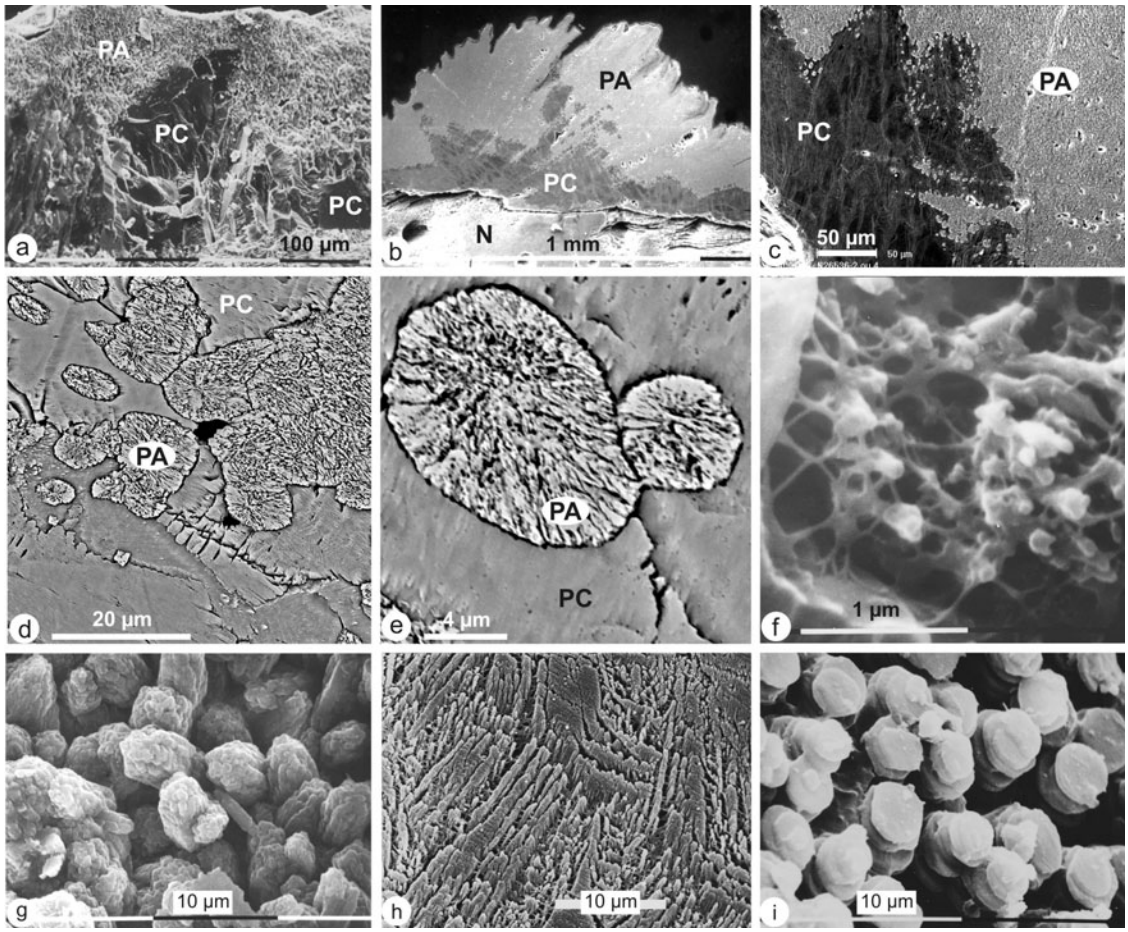

Figure 5. Microstructures of *Haliotis tuberculata*. **a:** Vertical fracture showing the inner calcitic patches (PC) and the outer aragonitic prismatic–spherulitic layer (PA). **b, c:** Polished, fixed, and etched surfaces showing the irregular arrangement of calcite and aragonite (PA) in the outer part of the shell; N: inner nacreous layer chromium sulfate for 90 s. **d, e:** Surface showing the microscale interplay between calcite and aragonite-polished, fixed, and etched surface, formic acid 0.1% + glutaraldehyde 3% for 25 s. Back scattered electron image. **f:** Fracture in the outer aragonitic layer showing the organic matrices as filaments. **g:** Fracture showing the small aragonitic units. **h:** Polished and etched surface showing the inner structure of the calcitic prisms fixed with glutaraldehyde for 30 min at 50°C, critical point drying. **i:** Columnar nacreous layer. PC, prismatic calcite; PA, prismatic–spherulitic aragonite; N, nacreous layer.

calcitic patches have a high content, whereas the nacre has a low content. This "sugar" map is very similar to that at 1,228 cm^{-1}, a wavelength related to SO_{42}– or amide III. Amide II (1,156 cm^{-1}) and amide I (1,607, 1,649 cm^{-1}) maps also show the differences in the organic components of the structures (Fig. 7). Amide I and the 1,720 cm^{-1} band (COOH) maps are similar. The 1,720 cm^{-1} band is strong in aspartic acid, an amino acid usually in high concentrations in biogenic carbonates.

Chemical Maps

Previous electron microprobe quantitative analyses and distribution maps have shown that despite seemingly higher Sr contents in aragonitic layers (nacre and prisms), the differences are not significant (Dauphin et al., 1989, 2007). The Mg content is more indicative of the mineralogy, especially in *H. tuberculata* (Fig. 8). As shown in Figure 8, the nacreous layer of *H. tuberculata* has the lowest Sr content, and the highest Mg content is found in the calcitic layer. Thus, Mg/Ca and Sr/Ca ratios in this species have been selected for chemical maps.

Using the NanoSIMS, more detailed distribution maps have been done in the outer layers, where aragonite and calcite were mixed. They clearly show the negative correlation between Mg and Sr in three mapped zones of *H. tuberculata* (Fig. 9). Mg/Ca maps are less distinct than those of Sr/Ca. Because of the irregular structures and thickness of the calcitic and aragonitic zones, it is difficult to know the actual origin of this phenomenon. However, Sr/Ca maps in the aragonite are not uniform (Fig. 9e). Detailed maps show aragonitic spherolites of about 1 μm in diameter (Figs. 9c, 9d).

Discussion

Electron microprobe analyses have previously shown that the shells of some *Haliotis* species comprise aragonite and calcite that are irregularly dispersed and mixed (Dauphin

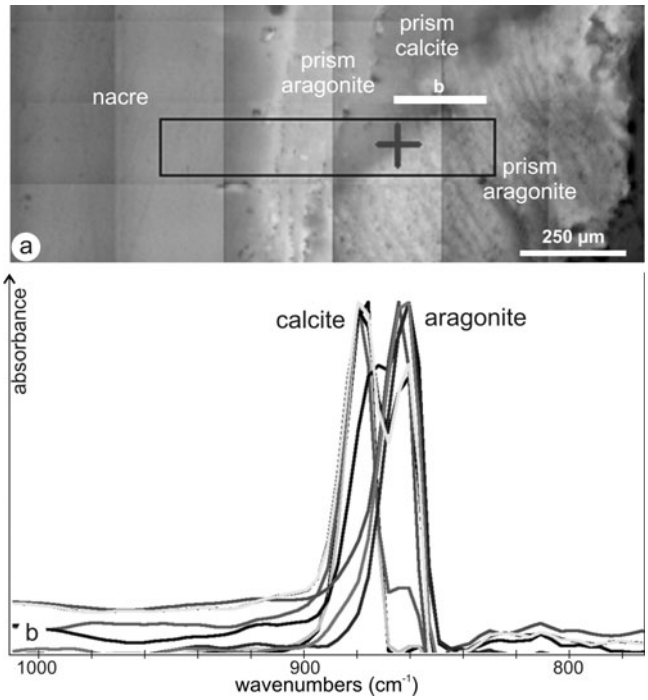

Figure 6. a: Polished surface showing the thick aragonitic nacreous layer, and the position of Fourier transform infrared microscopy maps (black rectangle) shown in Figure 7; the white line (**b**) corresponds to the spectra shown in (**b**) from calcite to aragonite. **b**: Spectra: IR absorption spectra showing the transition from aragonite to calcite extracted from the region labeled in the top optical image.

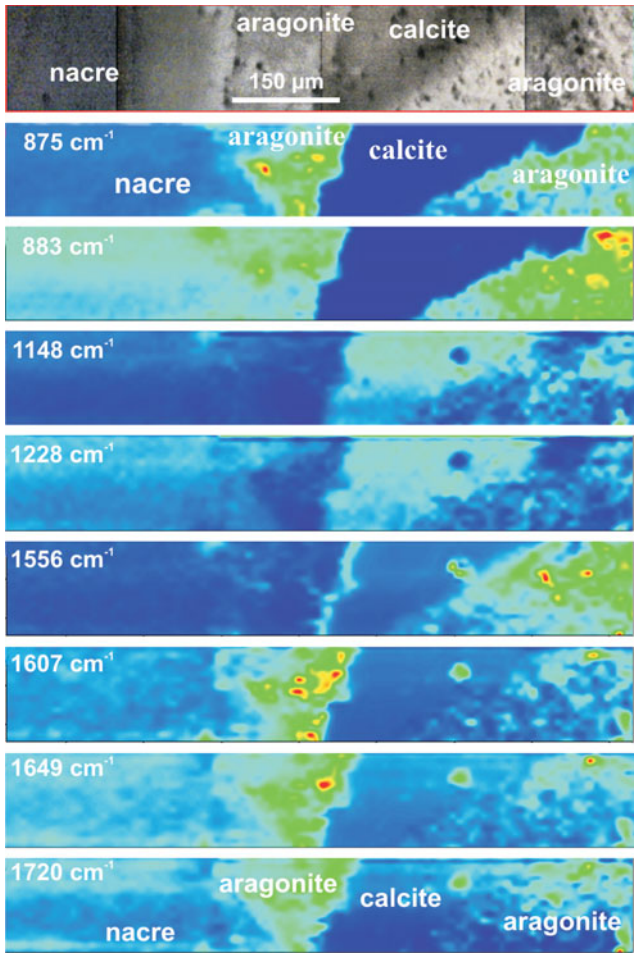

Figure 7. Top: Image of the mapped zone of the shell. Color images: Fourier transform infrared microscopy maps showing the compositional difference in mineralogy (875 cm^{-1}). Other maps show the differences in organic matrices between calcite and aragonite, and also between the aragonitic prismatic–spherulitic layer and the nacre.

et al., 2007). In regularly layered mollusk shells, a detailed examination of the boundary between the main layers shows transitional stages in both composition and structure (Dauphin et al., 2008, 2012; Farre et al., 2011; Nouet et al., 2012). In such shells, the main layers are easy to separate for various analyses, whereas the structure and composition of the transition layer is only known using *in situ* analyses. The efficiency of such techniques allows us to improve our knowledge of the complex and irregular shell of abalone.

The comparison of elemental chemical composition, fluorescence images, FTIR, and NanoSIMS maps shows the good correlation between structure mineralogy and biochemical composition at a microscale. The difference between the two types of aragonitic structures (nacre-prisms) is also confirmed.

In shells with more typical structure (two main layers), growth lines show that the mantle is able to produce simultaneously two different mineralizing organic matrices, with a transitional stage. In the most studied model (nacre-prism), the macromolecular assemblage for the prisms is first formed, then the nacreous macromolecular assemblage is done. There is no reverse production, from nacre to prism in these shells. In the prismatic layer, the presence of calcite and aragonite is not rare but the ratio calcite/aragonite is highly variable according to the species (Dauphin et al., 1989). Calcitic prisms are always larger than aragonitic units.

Some proteins have been localized in the mantle cells. According to these data, "cell clusters in the front edge of the mantle could be able to synthesize both aragonite and calcite matrix proteins" (Jolly et al., 2004). However, the growth-regulating mechanisms for such complex arrangements are not yet deciphered. Changes in mineralogy, crystallinity, and structure are normal in mollusks, but they usually follow a well-defined sequence. Nevertheless, the distribution of proteins probably involved in the biomineralization processes is both time and location dependent in *H. tuberculata* (Jardillier et al., 2008; Auzoux-Bordenave et al., 2010).

Mixed structures and mineralogies have been obtained in experiments involving mollusk shell repair and regeneration (Muzii et al., 1966; Saleuddin & Wilbur, 1969; Meenakshi et al., 1973, 1975; Chan & Saleuddin, 1974; Uozumi & Suzuki, 1979; Reed-Miller, 1983). In most cases, the structure and mineralogy of the repaired shells do not correspond to those of the normal shell. The first stages do not involve mineral deposits. Moreover, the organic contents of

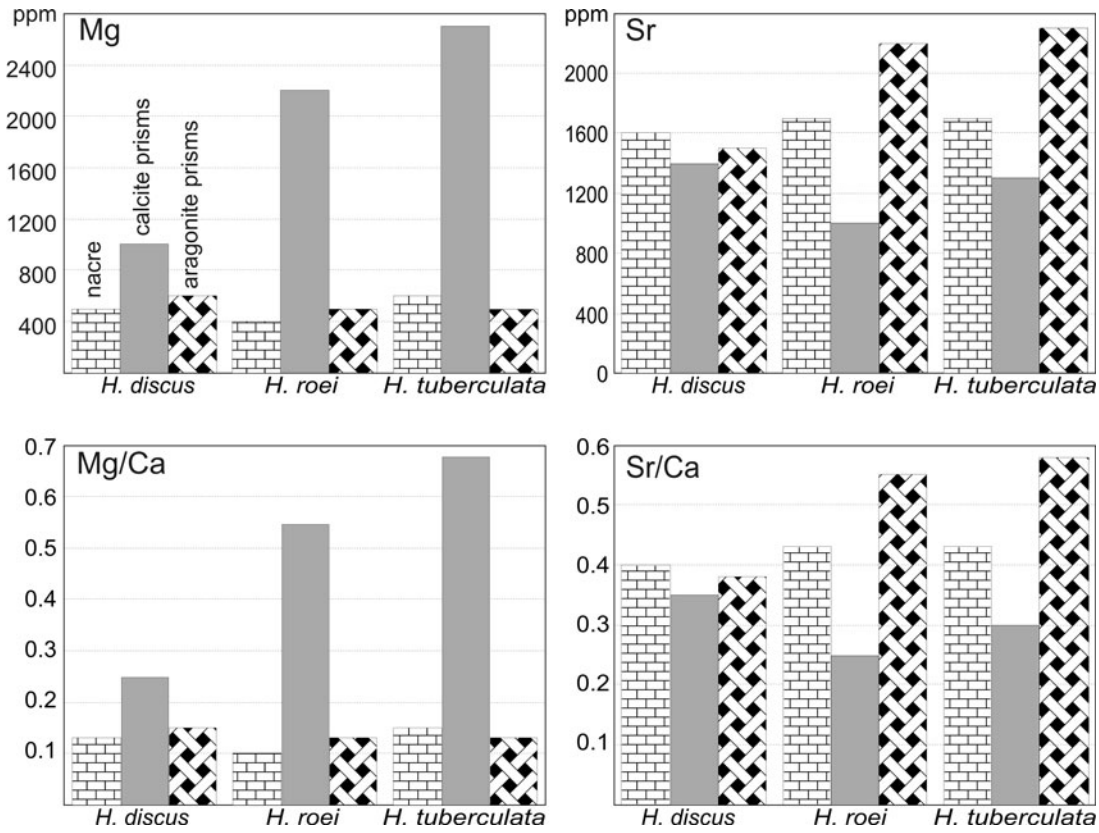

Figure 8. Elemental chemical composition (Mg, Sr) of the three structures in three species of *Haliotis*. Despite the common mineralogy (aragonite), nacre, and spherulitic–prismatic layers are not identical; 883 cm^{-1} band is assigned to C–H and CH_2 bonds, 1,148 cm^{-1} to sugars, 1,228 cm^{-1} to SO_4^{2-} or amide III, 1,156 cm^{-1} to amide II, 1,607 cm^{-1} and 1,649 cm^{-1} to amide I, and 1,720 cm^{-1} to aspartic acid.

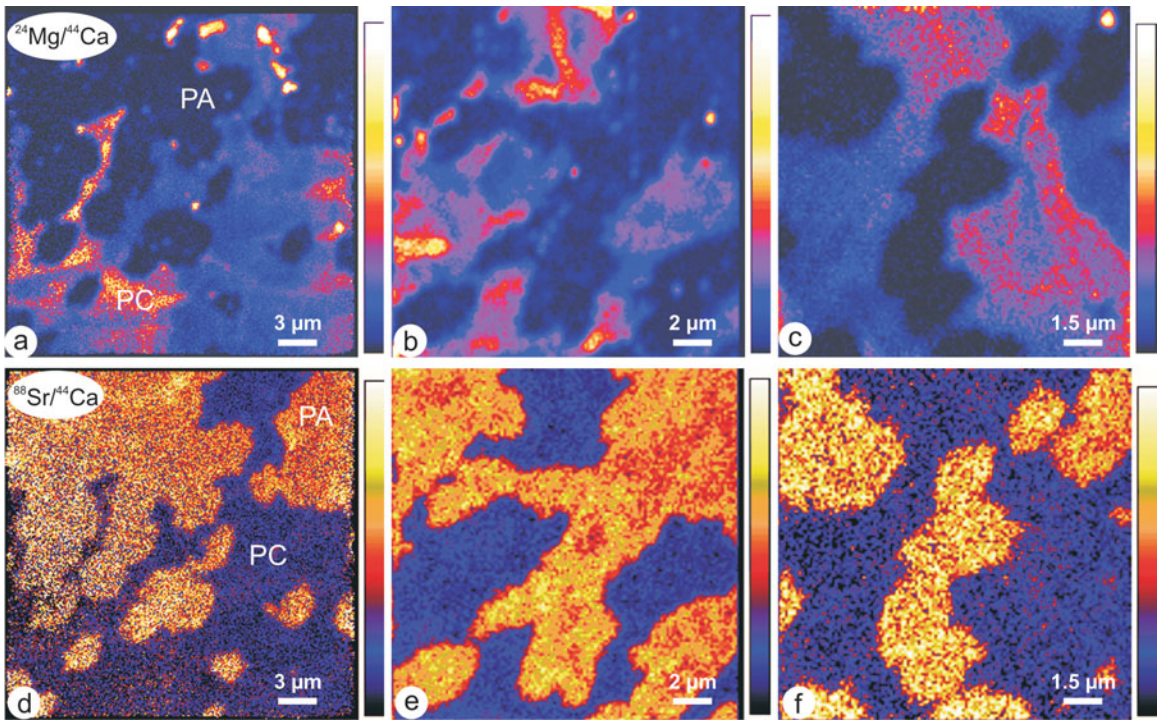

Figure 9. NanoSIMS images showing the microscale interplay between the prismatic calcite (high Mg/Ca) and the spherulitic aragonite (high Sr/Ca) in three different zones of the outer layers. PA, prismatic aragonite; PC, prismatic calcite.

the regenerating membrane are unusual, and cellular activities are higher. Meenakshi et al. (1974) observed that the repaired shell of a given species is dependent on the substrata inserted in the damaged zone. While structure and mineralogy are mixed throughout the life in the normal shell of *H. tuberculata*, shell repair is a sequential process.

Complex and irregular structures have been also described in cultured pearls (Cuif et al., 2011). As for regeneration experiments, irregularities are said to be the results of the stress induced by the grafting process: the small piece of mantle cut in another oyster, incision of the gonad to insert the nucleus and the mantle tissue. Moreover, in cultured pearls, the final structure is, in the end and in most cases, the nacreous layer.

Conclusion

The shell of *H. tuberculata* is irregularly layered: the inner layer is the aragonitic nacre, but the outer part of the shell is a mixture of prismatic calcite and spherulitic–prismatic aragonite. Such microscale mixings are unique in mollusk shells. Previous observations have shown that the structure, mineralogy, and elemental composition of these three phases differ. In such samples devoid of regular layers, only *in situ* analyses are available because of the complex arrangement and small sizes of the structural units. Additional analyses using confocal microscopy and infrared spectrometry maps at a microscale show that the organic components of these three phases differ. These results are concordant with what is known from other mollusks, the shell layers of which are easy to separate. Moreover, NanoSIMS chemical maps show that the chemical contents of the aragonite patches embedded in the calcite are not homogeneous. Again, similar results have been observed between two layers with different mineralogy in regularly layered mollusk shells. Thus, whatever the scale of observation, changes in the mineralizing process of the mantle cells are always progressive. The change in the secretion process from calcite to aragonite layers was estimated at ~6 days (Dauphin et al., 2008). In *Haliotis*, the physiological changes in the mantle cells must be faster, the size of the aragonitic patches being small (sometimes 1 μm). Throughout the lifespan of *Haliotis*, it seems that the same cells are able to synthesize and to very quickly switch from matrix components inducing calcite and aragonite.

Acknowledgments

This work was supported by ESRF Grant (EC 792) and by European Research Council Advanced Grant 246749 BIOCARB.

References

Auzoux-Bordenave, S., Badou, A., Gaume, B., Berland, S., Helléouet, M.N., Millet, C. & Huchette, S. (2010). Ultrastructure, chemistry and mineralogy of the growing shell of the European abalone *Haliotis tuberculata*. *J Struct Biol* **171**, 277–290.

Boggild, O.B. (1930). The shell structure of the molluscs. *D Kgl Danske Vidensk Selsk Skr, naturvidensk og mathem* **9**(2), 231–326.

Brahmi, C., Meibom, A., Smith, D.C., Stolarski, J., Auzoux-Bordenave, S., Nouet, J., Doumenc, D., Dejiat, C. & Domart-Coulon, I. (2010). Skeletal growth, ultrastructure and composition of the azooxanthellate scleractinian coral *Balanophyllia regia*. *Coral Reefs* **29**, 175–189.

Chan, J.F.Y. & Saleuddin, A.S.M. (1974). Acid phosphatase in the mantle of shell-regenerating snail *Helisoma duryi duryi*. *Calc Tiss Res* **15**, 213–220.

Clavier, J. (1982). Premières données sur les stocks naturels d'Ormeaux de la région de St. Malo. Association pour la mise en valeur du littoral de la côte d'émeraude, unpublished report, 100 pp.

Cuif, J.P., Dauphin, Y., Howard, L., Nouet, J., Rouzière, S. & Salomé, M. (2011). Is the pearl layer a reversed shell? A re-examination of the theory of pearl formation through physical characterizations of pearl and shell developmental stages in *Pinctada margaritifera*. *Aquat Living Resour* **24**, 411–424.

Dauphin, Y., Ball, A.D., Cotte, M., Cuif, J.P., Meibom, A., Salomé, M., Susini, J. & Williams, C.T. (2008). Structure and composition of the nacre-prism transition in the shell of *Pinctada margaritifera* (Mollusca, Bivalvia). *Anal Bioanal Chem* **390**, 1659–1669.

Dauphin, Y., Cuif, J.P., Cotte, M. & Salomé, M. (2012). Structure and composition of the boundary zone between aragonitic crossed lamellar and calcitic prism layers in the shell of *Concholepas concholepas* (Mollusca, Gastropoda). *Inverteb Biol* **131**, 165–176.

Dauphin, Y., Cuif, J.P., Mutvei, H. & Denis, A. (1989). Mineralogy, chemistry and ultrastructure of the external shell layer in ten species of *Haliotis*, with reference to *H. tuberculata* (Mollusca, Archaeogastropoda). *Bull Geol Inst Univ Uppsala NS* **15**, 7–38.

Dauphin, Y., Cuif, J.P., Salomé, M. & Susini, J. (2005). Speciation and distribution of sulfur in a mollusk shell as revealed by *in situ* maps using X-ray absorption near-edge structure (XANES) spectroscopy at the S K-edge. *Am Mineral* **90**, 1748–1758.

Dauphin, Y., Williams, C.T., Salomé, M., Susini, J. & Cuif, J.P. (2007). Microstructures and compositions of multilayered shells of *Haliotis* (Mollusca, Gastropoda). In *Biomineralization: From Paleontology to Materials Science, Proc 9th Inter Symp Biomin*, Arias, J.L. & Fernandez, M.S. (Eds.), pp. 265–272. Chile: University of Santiago.

Farre, B., Brunelle, A., Laprévote, O., Cuif, J.P., Williams, C.T. & Dauphin, Y. (2011). Shell layers of the black-lip pearl oyster *Pinctada margaritifera*: Matching microstructure and composition. *Comp Biochem Physiol B* **159**, 131–139.

Jardillier, E., Rousseau, M., Gendron-Badou, A., Fröhlich, F., Smith, D.C., Martin, M., Helléouet, M.N., Huchette, S., Doumenc, D. & Auzoux-Bordenave, S. (2008). A morphological and structural study of the larval shell from the abalone *Haliotis tuberculata*. *Mar Biol* **154**, 735–744.

Jolly, C., Berland, S., Millet, C., Borzeix, S., Lopez, E. & Doumenc, D. (2004). Zonal localization of shell matrix proteins in mantle of *Haliotis tuberculata* (Mollusca, Gastropoda). *Mar Biotechnol* **6**, 541–551.

Kessel, E. (1935). Über den bau der *Haliotis*-Schale. *Zool Anzeiger* **112**, 290–299.

Kopp, C., Meibom, A., Beyssac, O., Stolarski, J., Djediat, S., Szlachetko, J. & Domart-Coulon, I. (2011). Calcareous sponge biomineralization: Ultrastructural and compositional heterogeneity of spicules in *Leuconia johnstoni* Carter 1871. *J Struct Biol* **173**, 99–109.

Meenakshi, V.R., Blackwelder, P.L., Hare, P.E., Wilbur, K.M. & Watabe, N. (1975). Studies on shell regeneration-I. Matrix and mineral composition of the normal and regenerated shell of *Pomacea paludosa*. *Comp Biochem Physiol A* **50**, 347–351.

Meenakshi, V.R., Blackwelder, P.L. & Wilbur, K. (1973). An ultrastructural study of shell regeneration in *Mytilus edulis* (Mollusca: Bivalvia). *J Zool* **171**, 475–484.

Meenakshi, V.R., Donnay, G., Blackwelder, P.L. & Wilbur, K.M. (1974). The influence of substrata on calcification patterns in molluscan shell. *Calc Tiss Res* **15**, 31–44.

Meibom, A., Cuif, J.P., Hillion, F., Constantz, B.R., Juillet-Leclerc, A., Dauphin, Y., Watanabe, T. & Dunbar, R.B. (2004). Distribution of magnesium in coral skeleton. *Geophys Res Lett* **31**, doi:10.1029/2004GL021313.

Meibom, A., Cuif, J.P., Houlbrèque, F., Mostefaoui, S., Dauphin, Y., Meibom, K.L. & Dunbar, R. (2008). Compositional variations at ultra-structure length scales in coral skeleton. *Geochim Cosmochim Acta* **72**, 1555–1569.

Mutvei, H., Dauphin, Y. & Cuif, J.P. (1985). Observations sur l'organisation de la couche externe du test des *Haliotis* (Gastropoda): Un cas exceptionnel de variabilité minéralogique et microstructurale. *Bull Mus Natl Hist Nat Paris*, 4è sér, **7**(A1), 73–91.

Muzii, E.O., Catherine, H. & Skinner, W. (1966). Calcite deposition during shell repair by the aragonitic gastropod *Murex fulvescens*. *Science* **151**, 201–203.

Nouet, J., Cotte, M., Cuif, J.P., Dauphin, Y. & Salomé, M. (2012). Biochemical change at the setting-up of the crossed-lamellar layer in *Nerita undata* (Mollusca, Gastropoda). *Minerals* **2**, 85–99.

Reed-Miller, C. (1983). Scanning electron microscopy of the regenerated shell of the marine archaeogastropod. *Tegula Biol Bull* **165**, 723–732.

Saleuddin, A.S.M. & Wilbur, K.M. (1969). Shell regeneration in *Helix pomatia*. *Can J Zool* **47**, 51–53.

Taylor, J.D., Kennedy, W.J. & Hall, A. (1969). The shell structure and mineralogy of the Bivalvia. I. Introduction. Nuculacae-Trigonacae. *Bull Br Mus (Nat Hist) Zool* **3**, 1–125.

Uozumi, S. & Suzuki, S. (1979). "Organic membrane-shell" and initial calcification in regeneration. *J Fac Sci Hokkaido Univ*, ser 4, *Geol Miner* **19**, 37–74.

White, W.B. (1974). The carbonate minerals. In *The Infrared Spectra of Minerals*, Farmer, V.C. (Ed.), pp. 227–283. London: Mineralogical Society.